Broadband ultra-low-loss mesh filters on flexible cyclic olefin copolymer films for terahertz applications

F. Pavanello, F. Garet, M.B. Kuppam, Emilien Peytavit, M. Vanwolleghem, Francois Vaurette, J.L. Coutaz, Jean-Francois Lampin

Applied Physics Letters

Broadband ultra-low-loss mesh filters on flexible cyclic olefin copolymer films for terahertz applications

Cite as: Appl. Phys. Lett. **102**, 111114 (2013); https://doi.org/10.1063/1.4798522
Submitted: 01 February 2013 • Accepted: 14 March 2013 • Published Online: 22 March 2013

Fabio Pavanello, Frédéric Garet, Mohan-Babu Kuppam, et al.

AIP Publishing

Broadband ultra-low-loss mesh filters on flexible cyclic olefin copolymer films for terahertz applications

Fabio Pavanello,[1,a)] Frédéric Garet,[2] Mohan-Babu Kuppam,[2] Emilien Peytavit,[1] Mathias Vanwolleghem,[1] François Vaurette,[1] Jean-Louis Coutaz,[2] and Jean-François Lampin[1]
[1]*IEMN, UMR CNRS 8520, Avenue Poincaré, CS 60069, 59652 Villeneuve d'Ascq cedex, France*
[2]*IMEP-LAHC, UMR CNRS 5130, Université de Savoie, Site de Chambery Bâtiment Chablais, 73376 Le Bourget du Lac cedex, France*

(Received 1 February 2013; accepted 14 March 2013; published online 22 March 2013)

The cyclic olefin copolymer (COC) has recently demonstrated promising properties for THz applications due to its extremely high transparency in the THz region. Here, we prove that COC can be efficiently used as substrate material for free-space THz devices through the design, fabrication, and characterization of high-pass metal mesh filters. Measurements are in good agreement with calculations, and a transmittance higher than 75% has been measured between 1.5 THz and 2.5 THz for a single-layer filter. In addition, we prove that stacked meshes can be easily embedded to improve their rejection ratio in the stop-band, while preserving a high transparency in the pass-band. The broadband behavior of these filters should extend up to their diffraction limit estimated at around 6.3 THz for the single-layer filter. © *2013 American Institute of Physics*. [http://dx.doi.org/10.1063/1.4798522]

The cyclic olefin copolymer (COC)[1] is a promising dielectric material with unique properties, such as low water absorption, high chemical resistance, good metal adhesion, flexibility, low permittivity, and high transparency in the visible, UV, and THz region (0.1–10 THz).[2,3] All these properties are very attractive for various THz applications, added to the fact that polymers can be processed using standard photolithographic techniques.

Until now, polypropylene (PP) and benzocyclobutene (BCB) have been widely employed for free-space THz devices[4–7] due to their low absorption coefficient in the THz region ($\alpha = 2\,\mathrm{cm}^{-1}$ and $2.3\,\mathrm{cm}^{-1}$, respectively, at 1 THz).[8,9] Nevertheless, they present various drawbacks associated to some of their processing steps. On one side, PP films are only commercially available under specific film thicknesses, thus introducing design constraints. In addition, as recently observed for the fabrication of 3-D metamaterials, they may present a rough surface (granule size of 6–10 μm) that limits the maximal pattern resolution.[4] On the other side, spin-on BCB films require a hard-bake at 250 °C for 1 h under nitrogen atmosphere.[9] Induced stresses due to a different thermal expansion coefficient between BCB film and carrier substrate can affect the mechanical properties of the film, once removed from the host substrate.[10] Furthermore, it has been shown that a slight oxygen contamination during the hard-bake changes drastically BCB electrical properties.[9] In contrast, COC films can be obtained by spin coating of an appropriate commercial resin to achieve the desired thickness, while requiring a soft-bake at 140 °C for a few minutes.[11] Moreover, their absorption coefficient ($\alpha = 0.2\,\mathrm{cm}^{-1}$ at 1 THz) is nearly an order of magnitude lower than in the case of PP and BCB films.

COC has been already employed in several applications like THz fibers, low-loss interconnects, microfluidic devices, and waveguides.[2,11–13] However, despite these encouraging results, there is still no application of COC thin films (order of μm) as substrates for free-space THz devices. Mesh filters, metamaterials, and photonic band gap structures are only a few examples of applications where a low-loss substrate is essential to improve the overall performances.[14–16]

In this Letter, we investigate COC films as substrates for free-space THz devices through the fabrication of high-pass mesh filters with a cut-off frequency $f_{-3\mathrm{dB}}$ at 1 THz and a transmittance (referred to the power) higher than 75% over a broad range above 1.5 THz. This type of filters can be for instance placed in front of a bolometric detection system to filter out unwanted low frequency-harmonic signals that could arise from multiplier based THz frequency source or amplified spontaneous emission that could arise from photomixer based THz frequency source.[17,18] It can also be used to improve the sideband suppression ratio of a receiver system.[19] The low levels of power generated by photomixers at THz frequencies (order of μW) imply that such filters need to be transparent and broadband enough to maintain the source tenability.[20]

Mesh filters have been extensively investigated since the pioneering work by Ulrich due to their application as infrared filters for astronomy.[21] They have also been employed as polarizers, beam splitters, and reflectors in several domains like imaging, detection, or sensing.[16,21,22] In particular, high-pass filters can be free-standing (only the metal mesh) or substrate-based (the metal mesh lies on a substrate) crossed-mesh metallic patterns as shown in Fig. 1. Free-standing filters are characterized by a considerable thickness (tens of μm) for mechanical reasons, whereas substrate-based ones have metal thicknesses as small as hundreds of nm.[23] The EM response of these filters can be described in the framework of a coupled-mode theory.[24] Free-standing mesh filters cannot be highly transparent for evanescent modes due to their thickness t (a few μm thick is already detrimental

[a)]Electronic mail: fabio.pavanello@ed.univ-lille1.fr

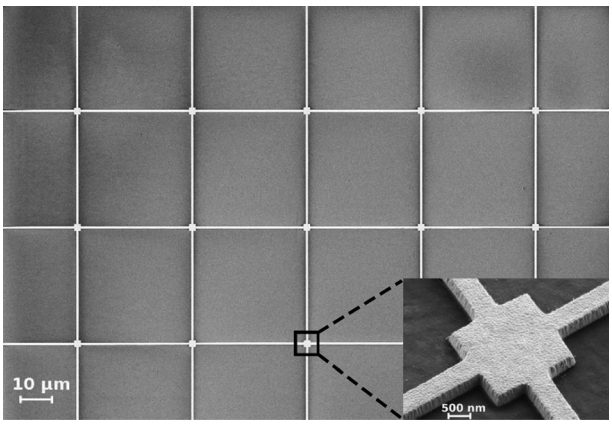

FIG. 1. SEM image of a single-layer filter before Si wafer removal. The lattice homogeneity (period of 38 μm) is well-maintained over the whole mesh surface. Inset: close-up of a mesh-cross, squares have been added to improve the adhesion and stability of the mesh wires (width of 500 nm) without influencing the EM response.

because of the exponential decay). The only solution is to make each aperture working as a classical waveguide, but the mesh aperture a has to be larger than 150 μm to allow transmission at frequencies higher than 1 THz. This reasoning implies that a high transparency over a broad bandwidth (larger than the mesh period d in wavelength) can be only achieved by a substrate-based filter. However, the substrate has to present low losses and permittivity and, at the same time, be well-suited to be processed by microelectronics techniques. In particular, the wire width w has to be as small as possible in order to decrease the reflection at the metal surface. Finally, a trade-off between all of these parameters has to be chosen to achieve f_{-3dB} at 1 THz. These considerations are also valid for a stacked structure but, due to a higher rejection ratio in the stop-band, d has to be larger than in the case of a single-layer filter. Here, the transmission properties of single-layer and double-layer filters are presented.

In order to obtain an accurate design taking into account effects like Fabry-Pérot fringes and/or losses in the substrate, a 3-D full-wave field simulation software (MICROWAVE STUDIO from CST) based on finite integration technique has been used.[14] Floquet's modes and infinite periodic boundary conditions have been chosen for the design to optimize the computing time and accuracy. The unit cells of the simulated structures are reported in Fig. 2. A lossy model (DC conductivity) for the metal mesh and an approximate 1st order Debye

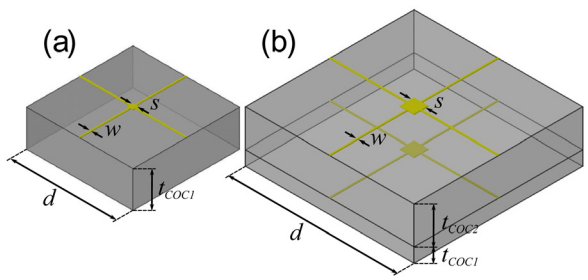

FIG. 2. Unit cells of the mesh-filters used for the simulations. Figs. 2(a) and 2(b) show the structures of the single-layer and double-layer filters, respectively. The structures are in scale and their dimensions are reported in Table I.

TABLE I. Parameters used in the design of the single-layer, the double-layer, and the triple-layer (only simulated) filters with f_{-3dB} at 1 THz (units are μm).

	d	w	s	t_{COC1}	t_{COC2}	t_{COC3}	t_{metal}
Single	38	0.5	2	13	…	…	0.31
Double	59	0.5	5	5	13	…	0.31
Triple	70	0.5	5	5	13	13	0.31

model for the substrate have been applied. In particular, the substrate permittivity is modeled by an algorithm using as input values a relative permittivity $\epsilon_r = 2.34$ and a tangent loss dielectric factor $\tan\delta = 2.3 \times 10^{-3}$ at 2.5 THz.[25] These parameters have been obtained by previous measurements of COC samples. The typical design of mesh filters has been slightly modified by adding a square block of side s at each mesh-cross (see Fig. 1). This element has no influence on the transmission properties for small s, but it is mechanically useful to keep the mesh well-aligned during the fabrication process, in particular when a new COC layer is deposited on top of it. In Table I, we summarize the parameters optimized by simulations for the fabricated single-layer and double-layer filters and the triple-layer (only simulated) filter.

The fabrication consists in COC[26] deposition by spin coating over an aluminum sacrificial layer onto a silicon substrate. Then, COC is cured at 140 °C for 2 min to obtain low stress films. Electron beam lithography is used for pattern definition due to the size of the smallest element ($w = 0.5$ μm).The size of w is a trade-off between the design and the fabrication constraints associated to the mesh stability and the possibility to use deep-UV lithography for cost effective fabrication process. Chrome (10 nm) and gold (300 nm) films are deposited by thermal evaporation followed by a lift-off technique. In the case of the double-layer structure, all of the fabrication steps are repeated. Finally, the filter is removed from the host substrate through a wet etching of the sacrificial layer and placed onto an annular holder as illustrated in Fig. 3. This fabrication process leads to high-quality lattices over large film surfaces (up to 2×2 cm^2 area) with metallic patterns characterized by a high definition as underlined in the inset of Fig. 1.

The measurements of the filters have been performed by THz time domain spectroscopy (THz-TDS) using a setup

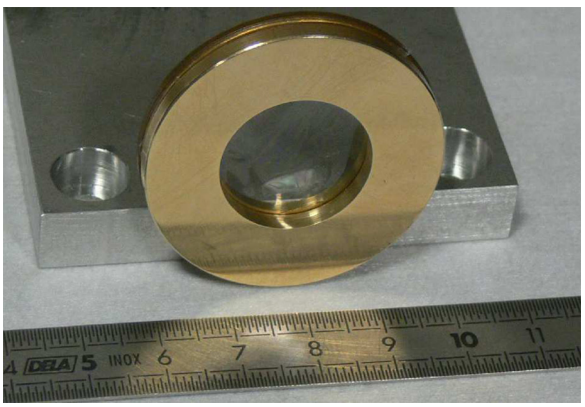

FIG. 3. Photograph of the single-layer filter mounted onto an annular holder. COC high transparency and sub-μm mesh wires width make the filter hardly visible.

based on low-temperature grown GaAs photoconductive switches illuminated by 100 fs-800 nm laser pulse for the emission and the detection of the signal. All of our spectra have been recorded under normal incidence, and no preferential polarization has been used due to the filter symmetry. Details of our setup and of the data post-processing can be found elsewhere.[27] A good agreement between simulation and measurements is observed for all devices. In particular, Fig. 4(a) underlines the key role of w in achieving high values of transmittance above 1.5 THz. A transmittance higher than 76% is obtained between 1.5 and 2.5 THz in the case of $w = 0.5\ \mu$m with f_{-3dB} at 1.02 THz. A rejection ratio of 13 dB/decade is achieved in the frequency range 0.25-2.5 THz. Main loss mechanisms in these filters are input and output coupling between plan wave and waveguide modes and destructive Fabry-Pérot fringes (for comparison, the film without the mesh presents a calculated transmittance of 90% at 2 THz). Metal reflections are negligible for $w = 0.5\ \mu$m because of the extremely thin mesh wires (the metal covers less than 3% of the overall surface). Finite metal conductivity at these frequencies is not a major cause of losses (for instance, a value of 0.12 dB higher can be obtained computationally for $w = 0.5\ \mu$m in a perfect electric conductor approximation at 2 THz).

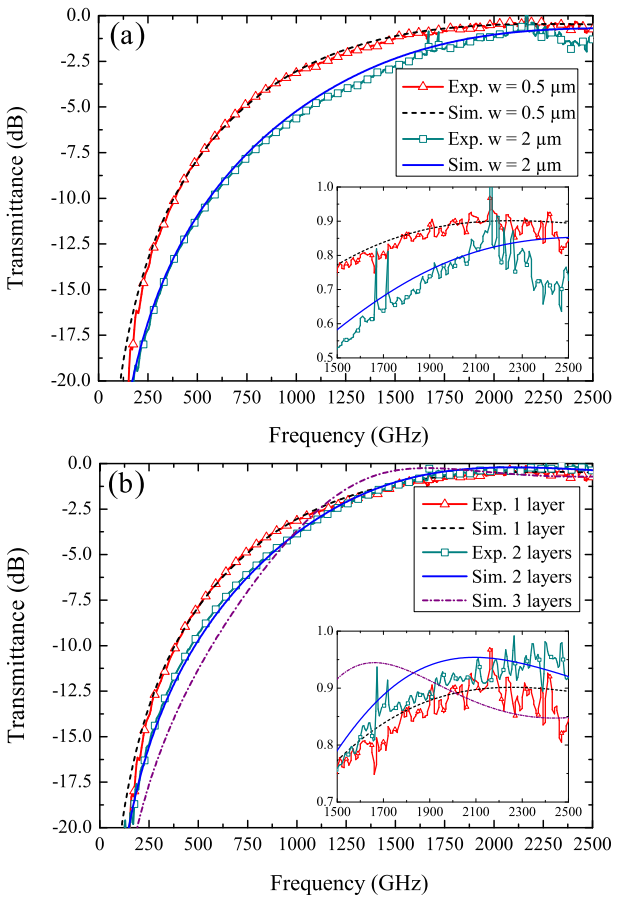

FIG. 4. Transmission properties of the mesh filters. Insets are in linear scale. Fig. 4(a) shows the comparison between two single-layer filters with different width w and same period $d = 38\ \mu$m. The inset reveals a higher transmittance above 1.5 THz for the filter with $w = 0.5\ \mu$m. Fig. 4(b) shows that multi-layer filters are able to increase the rejection ratio in the stop-band while keeping a high transmittance above 1.5 THz. The red curve (up triangle) and the black curve (dashed) have been reported as a reference and correspond to the same curves of Fig. 4(a). The inset emphasizes the role of Fabry-Pérot fringes in the pass-band.

Fig. 4(b) shows that a higher rejection ratio can be achieved in the stop-band when a stacked structure is used. Here, only two layers are considered but, as reported in the computational results, a structure with three layers would increase this effect. The double-layer filter has a measured rejection ratio of 15 dB/decade, while the 3-layers filter has a calculated rejection ratio of 17 dB/decade in the frequency range 0.25-2.5 THz. Computational results have shown that a larger dielectric spacing can be used to increase the rejection ratio, but a 13 μm thick dielectric spacing is used to achieve an accurate electronic alignment during the lithographic process. In all cases, the properties of COC are certainly critical to have low absorption in the substrate and low Fabry-Pérot fringes amplitudes.[14] It is worth noticing that the addition of layers to the structure forces to increase the mesh period to keep an f_{-3dB} at the same frequency due to the higher rejection ratio of stacked meshes. However, a larger period causes the diffraction to shift to lower frequencies, and thus, a low refractive index (effective for a thin substrate compared to the wavelength) is convenient to limit the amount of this shift.

In conclusion, we have shown that COC is a promising candidate for the next generation of free-space devices for THz applications due to its particularly suitable dielectric properties at these frequencies and to the possibility of fabricating accurate and reliable sub-μm metallic patterns, as demonstrated in this Letter. These features allow for the fabrication of robust, highly transparent broadband filters that can be integrated together with incoherent detection systems.

This work received financial support from the Seventh Framework Program for Research of the European Commission FP7/2007-2013 (Grant Agreement 238393—Marie-Curie initial training network "MITEPHO").

[1]Synthesized by Topas Advanced Polymer GmbH under the trade name of Topas™.
[2]K. Nielsen, H. K. Rasmussen, A. J. Adam, P. C. Planken, O. Bang, and P. U. Jepsen, Opt. Express **17**, 8592 (2009).
[3]P. D. Cunningham, N. N. Valdes, F. A. Vallejo, L. M. Hayden, B. Polishak, X.-H. Zhou, J. Luo, A. K.-Y. Jen, J. C. Williams, and R. J. Twieg, J. Appl. Phys. **109**, 043505 (2011).
[4]M. Navarro-Cía, S. A. Kuznetsov, M. Aznabet, M. Beruete, F. Falcone, and M. S. Ayza, IEEE J. Quantum Electron. **47**, 375 (2011).
[5]C. Croenne, F. Garet, E. Lheurette, J.-L. Coutaz, and D. Lippens, Appl. Phys. Lett. **94**, 133112 (2009).
[6]P. Weis, O. Paul, C. Imhof, R. Beigang, and M. Rahm, Appl. Phys. Lett. **95**, 171104 (2009).
[7]C. Jansen, S. Wietzke, V. Astley, D. M. Mittleman, and M. Koch, Appl. Phys. Lett. **96**, 111108 (2010).
[8]Y.-S. Jin, G.-J. Kim, and S.-G. Jeon, J. Korean Phys. Soc. **49**, 513 (2006).
[9]E. Perret, N. Zerounian, S. David, and F. Aniel, Microelectron. Eng. **85**, 2276 (2008).
[10]S. Bothra, M. Kellam, and P. Garrou, J. Electron. Mater. **23**, 819 (1994).
[11]E. Peytavit, C. Donche, S. Lepilliet, G. Ducournau, and J.-F. Lampin, Electron. Lett. **47**, 453 (2011).
[12]P. S. Nunes, P. D. Ohlsson, O. Ordeig, and J. P. Kutter, Microfluid. Nanofluid. **9**, 145 (2010).
[13]P. I. Okagbare, J. M. Emory, P. Datta, J. Goettert, and S. A. Soper, Lab. Chip **10**, 66 (2010).
[14]H. A. Smith, M. Rebbert, and O. Sternberg, Appl. Phys. Lett. **82**, 3605 (2003).
[15]H. Tao, A. C. Strikwerda, K. Fan, C. M. Bingham, W. J. Padilla, X. Zhang, and R. D. Averitt, J. Phys. D: Appl. Phys. **41**, 232004 (2008).

[16]S. Gupta, G. Tuttle, M. Sigalas, and K.-M. Ho, Appl. Phys. Lett. **71**, 2412 (1997).
[17]W. Li and J. Yao, IEEE Trans. Microwave Theory Tech. **58**, 3259 (2010).
[18]H. Song, N. Shimizu, T. Furuta, A. Wakatsuki, and T. Nagatsuma, Appl. Phys. Lett. **93**, 241113 (2008).
[19]I. S. Gregory, T. D. Drisdale, W. R. Tribe, D. R. S. Cumming, M. J. Evans, M. Missous, and E. H. Linfield, in *Joint 29th Int. Conf. on Infrared and Millimeter Waves and 12th Int. Conf. on Terahertz Electronics*, 27 September-1 October 2004, pp. 587–588.
[20]S. Preu, J. Appl. Phys. **109**, 061301 (2011).
[21]R. Ulrich, Infrared Phys. **7**, 37 (1967).
[22]S. Yoshida, E. Kato, K. Suizu, Y. Nakagomi, Y. Ogawa, and K. Kawase, Appl. Phys. Express **2**, 012301 (2009).
[23]P. A. R. Ade, G. Pisano, C. Tucker, and S. Weaver, Proc. SPIE **6275**, 62750U (2006).
[24]F. J. Garcia-Vidal, L. Martin-Moreno, T. W. Ebbesen, and L. Kuipers, Rev. Mod. Phys. **82**, 729 (2010).
[25]A. R. Djordjević, R. M. Biljić, V. D. Likar-Smiljanić, and T. K. Sarkar, IEEE Trans. Electromagn. Compat. **43**, 662 (2001).
[26]Grade T8007—Spin-on resin: mr-I T85-5.0 XP by micro resist technology.
[27]L. Duvillaret, F. Garet, and J. L. Coutaz, IEEE J. Sel. Top. Quantum Electron. **2**, 739 (1996).